Electronic Supplementary Material (ESI) for CrystEngComm.

A nacre protein forms mesoscale hydrogels that "hijack" the biomineralization process within a seawater environment. Supporting Information.

Martin Pendola,[1] Gaurav Jain,[1] Anastasia Davidyants,[1] Yu-Chieh Huang,[2] Denis Gebauer,[2] and John Spencer Evans[1] *

[1]Laboratory for Chemical Physics, New York University Center for Skeletal and Craniofacial Medicine, 345 E. 24th Street, NY, NY, 10010 USA.

[2]Department of Chemistry, Physical Chemistry, Universität Konstanz, Universitätstrasse 10, Konstanz D-78457, Germany.

*To whom correspondence should be addressed: Dr. John Spencer Evans, Center for Skeletal Sciences, Laboratory for Chemical Physics, New York University College of Dentistry, 345 E. 24th Street, New York, NY 10010 Telephone: (347) 753-1955; FAX: (212) 995-4087. E-mail: jse1@nyu.edu.

TABLE OF CONTENTS

I. Experimental

Sample preparation. The preparation and purification of chemically synthesized AP7 was performed as described previously.[1-7]

Micro-mineralization assays. Mineralization assays were adapted from published protocols[1-10] and were conducted by mixing equal volumes of 20 mM $CaCl_2$ * $2H_2O$, 100 mM $MgCl_2$, and 20 mM $NaHCO_3$ / Na_2CO_3 buffer to a final volume of 500 µL in sealed polypropylene tubes. The final assay concentrations were 50 mM $MgCl_2$, 10 mM $CaCl_2$, and 10 mM $NaHCO_3$ / Na_2CO_3 , with a final pH of the reaction solution in the range of 8.1 – 8.4. For precipitate collection clean 5 x 5 mm silicon wafer chips (TedPella, Inc., USA) were placed at the bottom of reaction vial for protein and mineral deposition capture. For negative control assays no protein solution was added; for AP7 assays, an appropriate microvolume (< 10 µL) of concentrated AP7 stock in unbuffered deionized distilled water was added to the appropriate vials to create a final AP7 assay concentration of 50 µM, which has been utilized in previous calcite-based mineralization assay studies.[1-3] Assay incubation times of 15, 30, and 60 min at room temperature were utilized. Upon completion of the mineralization assay period, the Si wafers were rinsed thoroughly with calcium carbonate saturated methanol and dried overnight at room temperature prior to analysis. For TEM studies, Formvar-coated Au TEM grids were glow discharged for 30 sec to remove the contaminants present on the film before sample application. Next, a 10 µL aliquot of the mineralization assay supernatant was withdrawn at the completion of the assay period, spotted onto these TEM grids, and washed and dried as described above.

Electron Microscopy. SEM imaging of the Si wafers extracted from the mineralization assays was performed using a Merlin (Carl Zeiss) field emission SEM using an Everhart-Thornley type secondary electron detector (SE2) at an accelerating voltage of 3-5 kV and a probe current of 100 pA. Prior to analysis, samples were coated with iridium (4 nm layer) using a Cressington 208HR sputter coater with thickness controller. X-ray microanalysis of the iridium coated Si wafers was performed using an Oxford Instruments EDS with integrated INCA software attached to the

Merlin FESEM. To perform the analysis, samples were lowered to a working distance of 8.5 mm and the acceleration voltage and probe current were increased to 5-7 kV and 1 nA, respectively, and areas of interests were scanned for 400 seconds each.

Transmission electron microscopy (TEM) imaging and electron diffraction analyses were performed using a Philips CM20 transmission electron microscope equipped with a LaB_6 filament electron beam source and 1024 x 1024 retractable CCD camera. All imaging and diffraction analyses were performed at 200 kV. A diffraction pattern of a polycrystalline gold standard was used as a calibration scale for all subsequently recorded diffraction patterns. The selected area diffraction (SAD) patterns were analyzed and indexed using CrysTBox software package.[11]

MicroRaman Microscopy. MicroRaman analysis of protein-deficient and AP7 mineralization assay samples as well as dried AP7 protein films on Si wafers were performed with a Thermo Scientific DXR Raman microscope. For the dried protein films, a 10 µL aliquot of 329 µM AP7 in Milli-Q pure water was spotted onto a clean 5 x 5 mm Si wafer chip and allowed to dry at room temperature for 2 hrs prior to analysis. Spectra were acquired under a 100X microscope objective with a laser excitation wavelength of 532 nm at 60-80% power (6-9 mW), 900 lines/mm grating, and a spot size of 0.7 µm. The spectra were processed using the OMNIC Atlus software designed for the instrument, using an aperture of 25 µm/pinhole, with 10 seconds exposure per sample.

Light microscopy. For detection of mesoscale protein hydrogel particles, 5 µL of a 50 µM AP7 in either 10 mM HEPES, 10 mM HEPES/10 mM $CaCl_2$, or 10 mM HEPES/10 mM $CaCl_2$/50 mM $MgCl_2$ (all pH 8.0) was placed on a clean glass slide with glass coverslip and imaged using bright field microscopy (40x or 60x objective, Nikon DS-U3 Light Microscope).

Flow cytometry experiments of AP7 protein aggregates. The aggregation of AP7 (50 µM final concentration) was studied under conditions of low ionic strength (10 mM HEPES, pH 8.0), in the presence of Ca(II)(10 mM HEPES, 10 mM $CaCl_2$, pH 8.0), which mimic the conditions utilized in standard calcite micromineralization assays,[1-5] and under seawater conditions (50 mM $MgCl_2$, 10 mM $CaCl_2$, 10 mM HEPES, pH 8.0) similar to those found our current 5:1 Mg(II):Ca(II) micromineralization assays. Carbonate and bicarbonate ions were omitted from these experiments since the formation of mineral particles would complicate protein particle interpretations. Samples were constituted and allowed to sit for 5 min prior to analysis. Aggregation measurements were performed using a multi-parameter cell analyzer CytoFLEX (Beckman Coulter, CA, USA). Each sample solution (100 µL) was analyzed at a continuous flow rate of 10 µL/min using four laser excitation lines of 405 nm, 488 nm, 561 nm, and 640 nm to register two light-scattering parameters (FSC-A and SSC-A)[12-15] and the number of events for each sample. Data was collected using the CytExpert 1.2.11.0 software designed for the instrument and processed using FlowJo software (TreeStar, OR, USA).

AFM Imaging. We investigated the morphological and quantitative characteristics of AP7 assemblies and nanoparticles captured onto mica substrates. The apo form (i.e., Ca^{2+} free) of 10 µM AP7 was imaged in 10 mM HEPES buffer (pH 8.0). In addition, we imaged 10 µM AP7 in 10 mM $CaCl_2$, 10 mM HEPES and 10 mM $CaCl_2$, 50 mM $MgCl_2$, 10 mM HEPES (pH 8.0) to

mimic conditions similar to those found in calcitic and aragonitic mineralization assays, respectively. AFM experiments were conducted at 25 °C using an Asylum MFP-3D-BIO instrument operating in tapping mode in a buffer solution. Bruker DNP-S triangular-shaped, silicon-nitride tips with a spring constant of approximately 0.12 N/m and a drive frequency varying in the range of › 50 kHz - 90 kHz to achieve the best image quality were used for imaging. All samples were aliquoted onto a freshly stripped surface of mica (0.9 mm thick, Ted Pella, Inc.) and incubated for a period of 15 min at ambient temperature prior to measurement. Images were acquired at a scan rate of 0.75 Hz. Gwyddion software was implemented for image processing, noise filtering, and analysis, including the calculation of R_q, i.e., the surface roughness of the imaging surface.

Ca/Mg potentiometric titrations. Potentiometric titration experiments[16,17] were conducted by utilizing a computer-controlled system manufactured by Metrohm. The setup is composed of two devices (Titrando 809 and Titando 905) controlling three dosing devices (800 Dosino) for dosing $CaCl_2$ (10 mM), NaOH (10 mM) and HCl (100 mM), respectively. One Ca^{2+}-selective electrode (Metrohm No. 6.0508.110) and one pH-electrode (Metrohm No. 6.0256.100) are utilized to monitor the calcium potential and pH, respectively. During a titration experiment, $CaCl_2$ (10 mM) is continually dosed into carbonate buffer (10 mM, 20mL) at a constant rate of 20 μL /min and the pH is kept constant at pH 8.5 by addition of NaOH and HCl. Here, HCl titration is required for balancing the outgassing of CO_2, which starts to become significant below pH 9.00.[17] The same method is applied for the magnesium titration experiments, but the $CaCl_2$ (10 mM) is replaced by the mixture of $CaCl_2$ (10 mM) and $MgCl_2$ (50 mM). For protein experiments, the potentiometric titrations are performed as described above, but in presence of AP7 protein in the carbonate buffer (500 nM or 1 μM final protein concentrations as indicated).

The standard potentiometric curve provides information on the formation and stabilities of PNCs in solution. As free Ca^{2+} or 5:1 Mg^{2+} : Ca^{2+} are is added to the carbonate solution, ion complexes (i.e., PNCs) form and this is represented by the initial linear region of the titration curve. Where the measured free Ca^{2+} decreases upon further addition of $CaCl_2$ (i.e., the peak region), this marks the start of solid phase nucleation (e.g., ACC) from PNCs. With respect to PNC stability, the slope of the prenucleation regime (i.e., the initial linear region) provides indirect evidence of the interaction between additive molecules and solute ion associates, leading to PNC stabilization (i.e., $Slope_{Additive} < Slope_{Ref}$) or destabilization ($Slope_{Additive} > Slope_{Ref}$).

II. Annotated AP7 flow cytometry graphs plots.

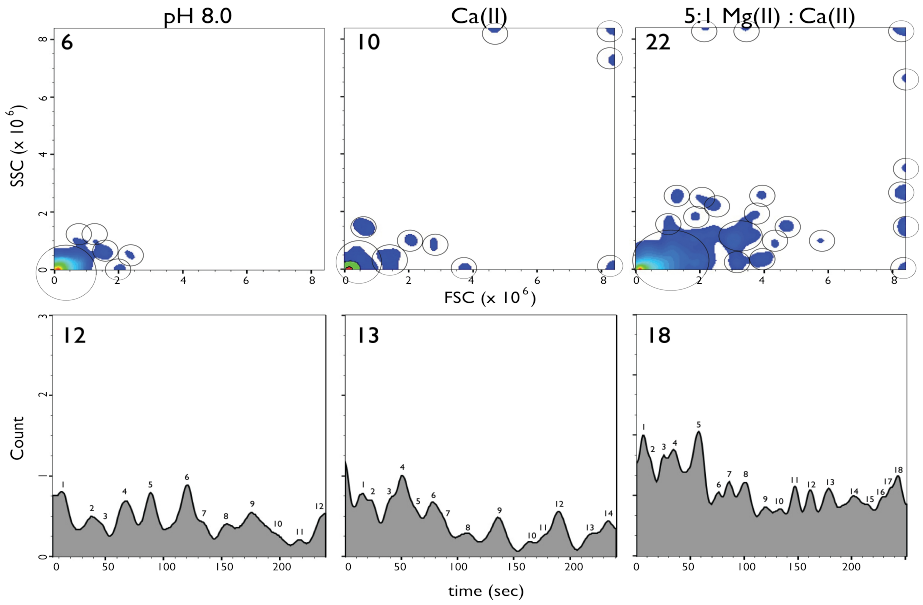

Figure S1. Annotated Flow cytometry 2-D density (TOP) and 1-D particle number as a function of flow time (BOTTOM). In 2-D plots, circled areas are resolvable FSC vs SSC populations of protein particles that we identified. In 1-D plots, peak and shoulder regions representing particle counts as a function of flow time are identified. Please refer to Fig 1 legend for details on sample conditions.

III. Tapping mode AFM imaging of AP7 protein phases under low ionic strength, Ca(II), and 5:1 Mg(II) : Ca(II) conditions, pH 8.0

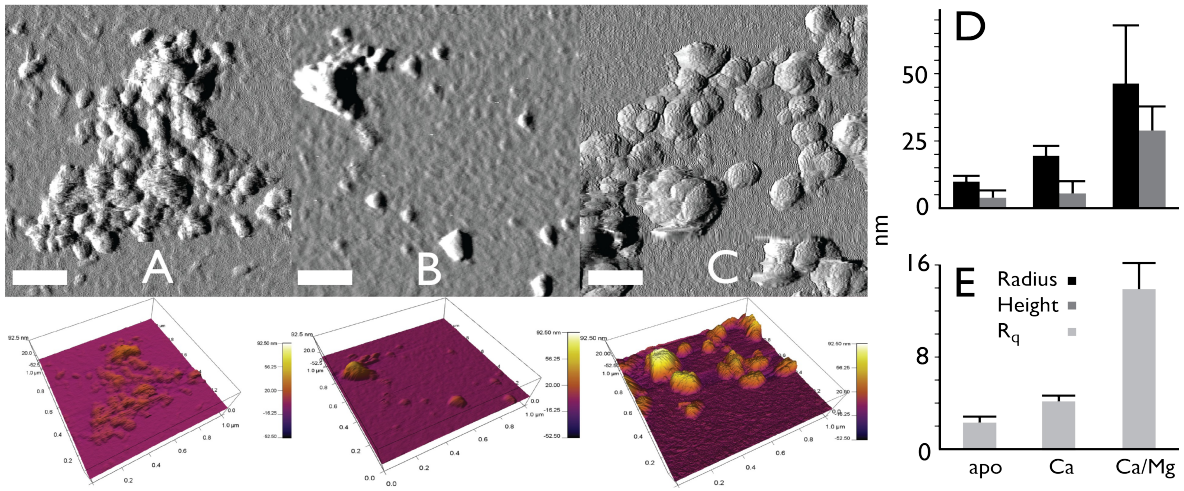

Figure S2. AFM tapping mode imaging datasets for 10 µM AP7. The amplitude (TOP) and height (BOTTOM) plots are of AP7 protein phases/hydrogels imaged on mica surfaces in (A) 10 mM HEPES, pH 8; (B) 10 mM HEPES, 10 mM $CaCl_2$, pH 8; (C) 10 mM HEPES, 10 mM $CaCl_2$, 50 mM $MgCl_2$, pH 8; (D) Histogram analysis of particle radii and heights taken from 30 measurements (± S.D.); Histogram analysis of R_q, or surface roughness parameter, taken from 30 measurements (± S.D.)

Discussion of results. In the apo-state (10 mM HEPES, pH 8.0) AP7 exhibits the typical amorphous-appearing individual and clustered protein particles that reside on top of a protein film layer, which is visible in the background coating the mica surface (Fig S2A). The presence of a protein layer is also confirmed by the R_q, or surface roughness parameter, which is 2.3 nm for the AP7 sample at pH 8 versus 0.034 nm for plain mica under identical buffer conditions. Relative to the apo condition, in the presence of Ca(II) we note that the protein particles increase in radii (2-fold) and heights (1.5-fold)(Fig S2B, D), as does the R_q (2-fold, Fig S2E), which indicates that Ca(II) ions increase aggregation propensity. But the most dramatic effects are observed in the presence of 5:1 Mg(II) : Ca(II), where the protein aggregation state clearly exceeds all other tested conditions (Fig S2C). Here, the particle radii, heights, and R_q values increase by a factor of 5, 7, and 6, respectively, from the apo-state (Fig S2D,E). Interestingly, under these conditions the composition of the protein phases changes, such that there is increased AFM tip interference with the protein, leading to imaging artifacts (Fig S2C, lower half of amplitude plot). Nonetheless, as we suspected, the 5:1 Mg(II) : Ca(II) environment promotes further AP7 aggregation propensity and these findings explain why AP7 deposition and protein phase/hydrogel formation predominate within our 5:1 Mg(II):Ca(II)-based microassay systems. (Figs 1,2). At this time it is not clear whether the increase in protein aggregation propensity is Mg(II) specific, or, is the result of higher ionic strength conditions inherent within 50 mM $MgCl_2$ / 10 mM $CaCl_2$ versus 10 mM $CaCl_2$ solutions.

IV. SEM imaging of Si wafer deposition in time-dependent 5:1 Mg(II):Ca(II) assays.

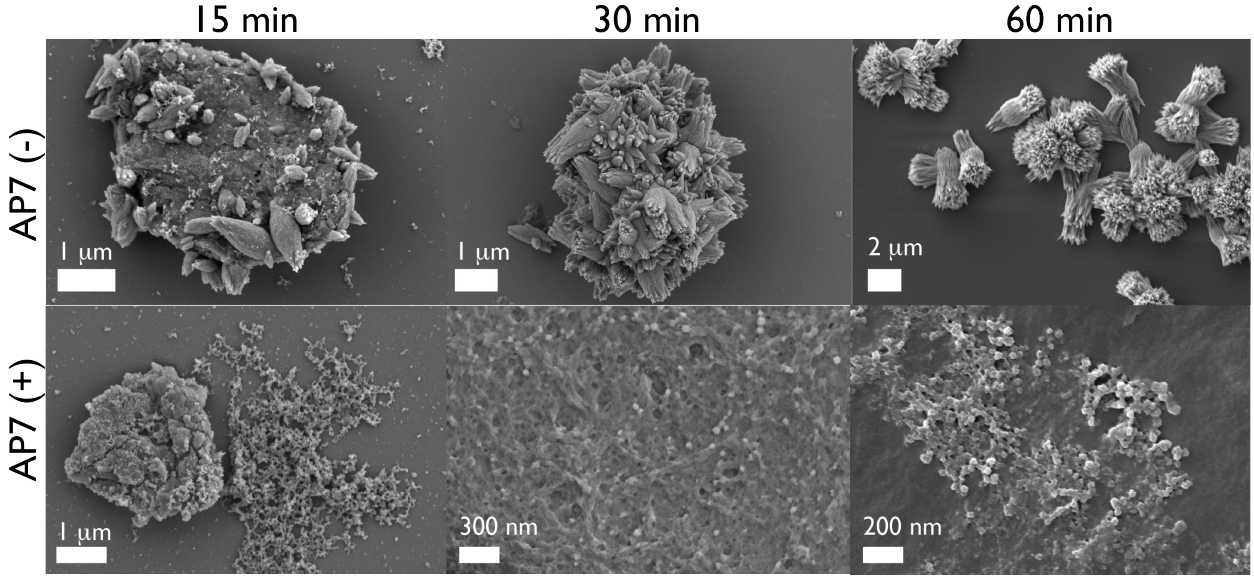

Fig S3. SEM images of Si wafer captured deposits taken from time-dependent Mg(II):Ca(II) 5:1 micromineralization assays. (-) AP7 = protein deficient negative controls; (+) AP7 = 50 μM AP7. In (-) AP7 controls, note mineral aggregates. In (+) AP7 assays, note extensive protein aggregation and the presence of individual mineral nanoparticles (30 min) and nanoparticle clusters (60 min) within the protein aggregates.

V. TEM imaging of rescued supernatant samples from time-dependent 5:1 Mg(II):Ca(II) assays.

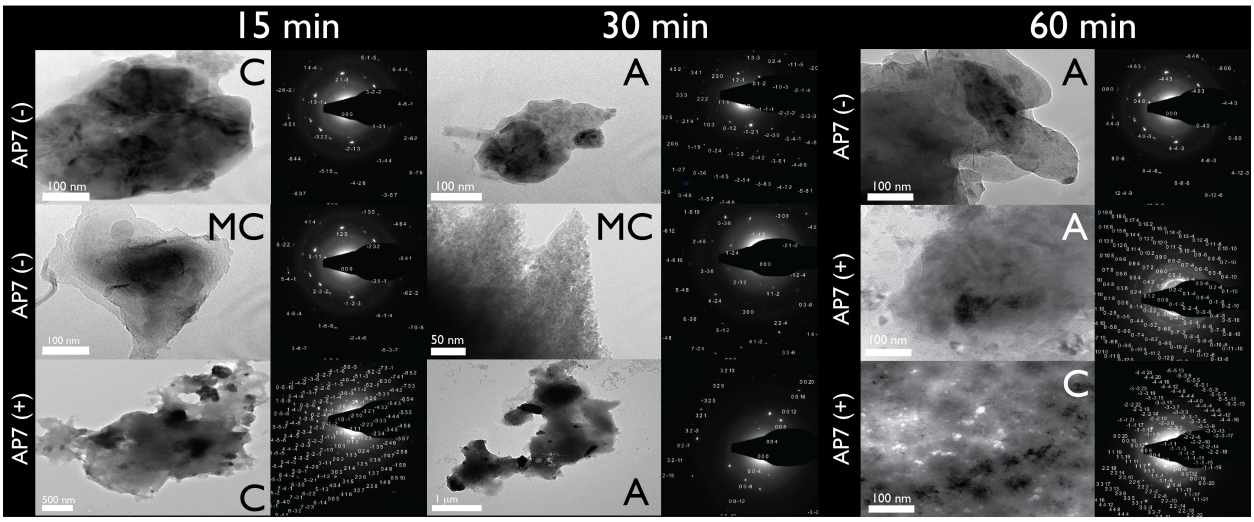

Fig S4. TEM images and corresponding annotated selected area diffraction patterns of supernatant samples rescued from time-dependent Mg(II):Ca(II) 5:1 micromineralization assays. (-) AP7 = protein deficient negative controls; (+) AP7 = 50 µM AP7. A = aragonite; C = calcite; MC = magnesium calcite. The selected area diffraction (SAD) patterns were analyzed and indexed using a standard Au sample and the CrysTBox software package.[18]

VI. X-ray powder diffraction spectra of protein-deficient 5:1 Mg(II):Ca(II) assays.

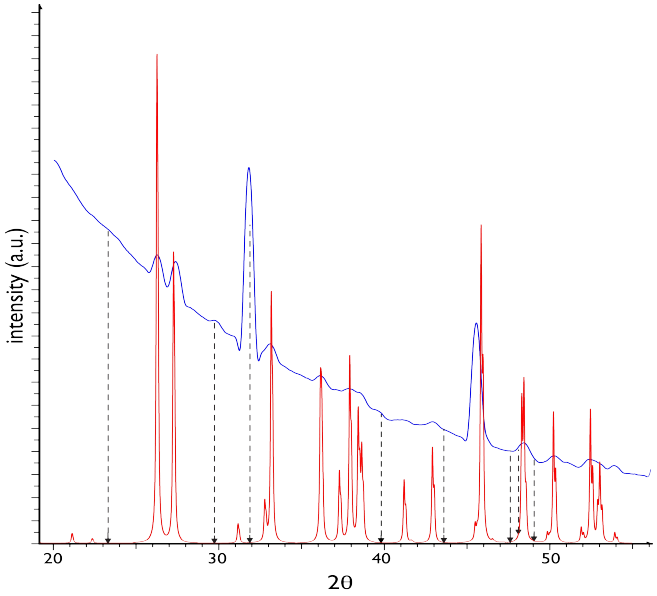

Fig S5. Powder X-ray diffraction spectra of mineral deposits collected on Si wafers from protein – deficient 5:1 Mg(II) : Ca(II) 60 min mineralization assays. Blue = assay sample spectra; red = simulated aragonite spectra; dashed lines = simulated magnesium calcite.

VII. X-ray microanalyses of protein-deficient controls and mineralized AP7 protein phases.

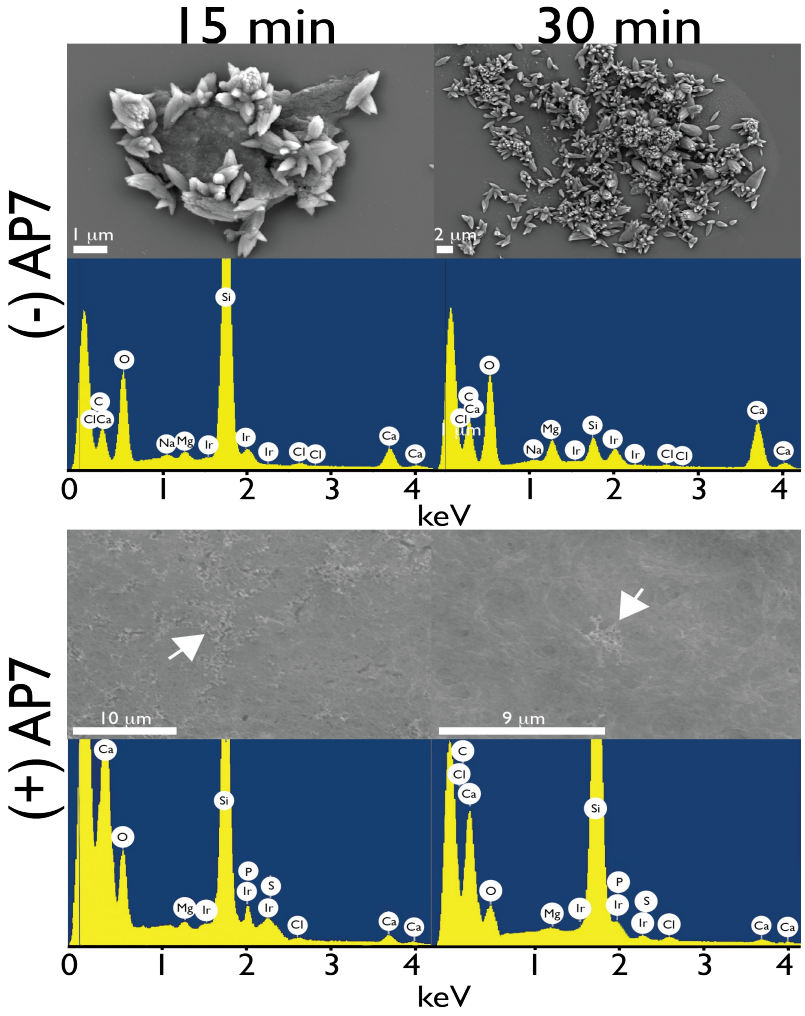

Fig S6. X-ray microanalyses and corresponding SEM images of crystals retrieved from protein deficient [(-) AP7] and 50 µM [(+) AP7] Mg(II):Ca(II) 5:1 15 and 30 min microassays. White arrows indicate sampling region for the (+) AP7 protein hydrogels Samples were coated with iridium (Ir) prior to imaging.

VIII. MicroRaman spectra of microassay deposits and dried AP7 protein films.

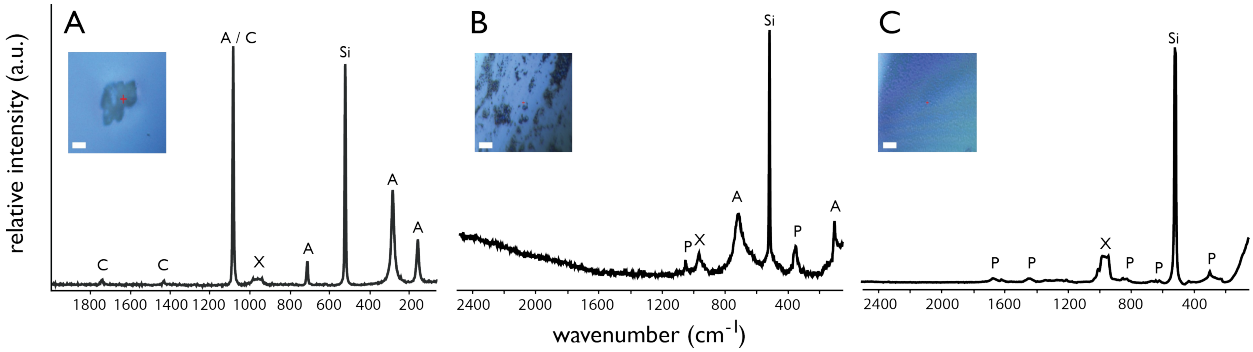

Fig S7. MicroRaman spectra. (A) Si wafer – captured deposits, protein-deficient 5:1 Mg(II):Ca(II) 60 min micromineralization assays, (B) Si wafer – captured deposits, 50 µM AP7 5:1 Mg(II):Ca(II) 60 min micromineralization assays, (C) dried AP7 protein films, created from 100 µL aliquot of 50 µM AP7 in Milli-Q deionized distilled water deposited onto Si wafer and dried at room temperature). Assignment of Raman bands: A= aragonite; C = calcite/magnesium calcite; P = protein specific; X = atmospheric amine contaminants. For each spectra, the corresponding sample light microscope image is shown (inset). Scalebars = 100 µm.

Table S1: Raman band assignments for $CaCO_3$ polymorphs

Mode	calcite	vaterite	aragonite
Lattice mode (cm^{-1})	156, 283	118, 268, 301	154, 208, 273
v_1, symmetric stretch (cm^{-1})	1086	1074, 1089	1086
v_2, out-of-plane bending (cm^{-1})	---	874	854
v_3, asymmetric stretch (cm^{-1})	1435	1445, 1485	1462, 1574
v_4, in-plane bending (cm^{-1})	713	738, 750	704, 717
Overtones (cm^{-1})	1749	1749	---

Taken from ref 19. Reported values are for synthetic calcium carbonates.

IX. Ca(II)/Mg(II) Potentiometric Titration Data

Table S2. Potentiometric Ca(II) titration data obtained for AP7 and reference (protein-deficient) samples, pH 8.5.

Sample	Pre-nucleation Slope (mol/s)	Nucleation time (s)	Solubility (M^2)
Reference (-) Mg	$2.49\times10^{-9} \pm 0.35\times10^{-11}$	9760 ± 720	$3.51\times10^{-8} \pm 3.04\times10^{-11}$
Reference (+) Mg	$2.70\times10^{-9} \pm 2.22\times10^{-11}$	15485 ± 2795	n/a[1]
500 nM AP7 (+) Mg	$2.76\times10^{-9} \pm 2.70\times10^{-11}$	48445 ± 4075	n/a[1]
1 µM AP7 (+) Mg	$2.85\times10^{-9} \pm 4.71\times10^{-11}$	No nucleation	No nucleation

The errors represent ± one standard deviation.

[1]The ion product keeps decreasing, i.e. no defined solubility threshold is established. This is likely due to the presence of Mg(II), that is, water and/or Mg(II) ions may be continuously expelled from the initially precipitated phase, changing its composition, stability, and hence, solubility. On the other hand, it may be a kinetic effect, e.g. inhibition of the inclusion of ions into a phase of a constant low solubility. Initially, the ion product is on the order of 5.75×10^{-8} M^2 and gradually decreases with time.

X. References

1. Chang, E.P., Williamson G., Evans, J.S. (2015) *Crystal Growth and Design 15,* 1577-1582.

2. Perovic, I., Chang, E.P., Verch, A., Rao, A., Cölfen, H., Kröger, R., Evans, J.S. (2014) *Biochemistry 53*, 7259-7268.

3. Chang, E.P., Russ, J.A., Verch, A., Kröger, R., Estroff, L.A., Evans, J.S. (2014) *Biochemistry 53*, 4317-4319.

4. Chang, E.P., Perovic, I., Rao, A., Cölfen, H., Evans, J.S. (2016) *Biochemistry 55*, 1024-1035.

5 . Chang, E.P., Roncal-Herrero, T., Morgan, T., Dunn, K.E., Rao, A., Kunitake, J.A.M.R., Lui, S., Bilton, M., Estroff, L.A., Kröger, R., Johnson, S., Cölfen, H., Evans, J.S. (2016) *Biochemistry 55*, 2401-2410.

6. Amos, F.F., Ndao, M., Ponce, C.B., Evans, J.S., (2011) *Biochemistry 50*, 8880-8887.

7. Amos, F.F, Ponce, C.B., Evans, J.S. (2011) *Biomacromolecules 12*, 1883-1890.

8. Chang, E.P., Russ, J.A., Verch, A., Kröger, R., Estroff, L.A., Evans, J.S. (2014) *Cryst.Eng. Commun. 16*, 7406-7409.

9. Chang, E.P., Evans, J.S. (2015) *Biochemistry 54*, 5348-5355.

10. Perovic, I., Chang, E.P., Lui, M., Rao, A., Cölfen, H., Evans, J.S. (2014) *Biochemistry 53*, 2739-2748.

11. Klinger, M., Jäger, A. (2015) *Journal of Applied Crystallography 48*, 2012-2018.

12. Cui, J., Bjornmalm, M., Liang, K., Xu, C., Best, J.P., Zhang, X., Caruso, F. (2014) *Adv. Materials 26*, 7295-7299.

13. Cho, S.H., Godin, J.M., Chen, C.-H., Qiao, W., Lee, H., Lo, Y.-H. (2010) *Biomicrofluidics 4*, 043001.

14. Patanaruta, A., Luchini, A., Botterell, P.J., Mohana, A., Longo, C., Vorstere, P., Petricoin, E.F. III, Liotta, L.A., Bishop, B. (2010) *Colloids and Surfaces A: Physicochemical and Engineering Aspects 362*, 8-19.

15. Henel, G., Schmitz, J.L. (2007) *Labmedicine 38*, 428-436.

16. Kellermeier, M., Cölfen, H., Gebauer, D. (2013) in Research Methods in Biomineralization Science. Ed. By De Yoreo, J.J. Book Series: *Methods in Enzymology 532*, 45-69.

17. Verch A, Antonietti M, Cölfen H (2012) *Z Krist - Cryst Mat 227*, 718–722.

18. Klinger, M., Jäger, A. (2015) *Journal of Applied Crystallography 48*, 2012-2018.

19. Ndao, M., Keene, E., Amos, F.A., Rewari, G., Ponce, C.B., Estroff, L.A., Evans, J.S. (2010) *Biomacromolecules 11*, 2539.